Macrophage-mediated delivery of light activated nitric oxide prodrugs with spatial, temporal and concentration control† †Electronic supplementary information (ESI) available: Includes detailed experimental details plus 10 additional figures. See DOI: 10.1039/c8sc00015h

Chemical Science

EDGE ARTICLE

View Article Online
View Journal | View Issue

Cite this: *Chem. Sci.*, 2018, **9**, 3729

Macrophage-mediated delivery of light activated nitric oxide prodrugs with spatial, temporal and concentration control†

Michael A. Evans,‡[abc] Po-Ju Huang,‡[a] Yuji Iwamoto,[d] Kelly N. Ibsen,[b] Emory M. Chan,[e] Yutaka Hitomi,[d] Peter C. Ford *[a] and Samir Mitragotri *[bc]

Nitric oxide (NO) holds great promise as a treatment for cancer hypoxia, if its concentration and localization can be precisely controlled. Here, we report a "Trojan Horse" strategy to provide the necessary spatial, temporal, and dosage control of such drug-delivery therapies at targeted tissues. Described is a unique package consisting of (1) a manganese–nitrosyl complex, which is a photoactivated NO-releasing moiety (photoNORM), plus Nd^{3+}-doped upconverting nanoparticles (Nd-UCNPs) incorporated into (2) biodegradable polymer microparticles that are taken up by (3) bone-marrow derived murine macrophages. Both the photoNORM $[Mn(NO)dpaq^{NO_2}]BPh_4$($dpaq^{NO_2}$ = 2-[*N*,*N*-bis(pyridin-2-yl-methyl)]-amino-*N*′-5-nitro-quinolin-8-yl-acetamido) and the Nd-UCNPs are activated by tissue-penetrating near-infrared (NIR) light at ~800 nm. Thus, simultaneous therapeutic NO delivery and photoluminescence (PL) imaging can be achieved with a NIR diode laser source. The loaded microparticles are non-toxic to their macrophage hosts in the absence of light. The microparticle-carrying macrophages deeply penetrate into NIH-3T3/4T1 tumor spheroid models, and when the infiltrated spheroids are irradiated with NIR light, NO is released in quantifiable amounts while emission from the Nd-UCNPs provides images of microparticle location. Furthermore, varying the intensity of the NIR excitation allows photochemical control over NO release. Low doses reduce levels of hypoxia inducible factor 1 alpha (HIF-1α) in the tumor cells, while high doses are cytotoxic. The use of macrophages to carry microparticles with a NIR photo-activated theranostic payload into a tumor overcomes challenges often faced with therapeutic administration of NO and offers the potential of multiple treatment strategies with a single system.

Received 2nd January 2018
Accepted 12th March 2018

DOI: 10.1039/c8sc00015h

rsc.li/chemical-science

Introduction

Nitric oxide (NO) has exhibited significant potential as a cancer therapy, but its effects are highly concentration- and location-dependent.[1] Furthermore, NO has a relatively short lifetime in physiological media and induces significant side effects when delivered systemically.[2] Targeting strategies must be a key feature for the delivery of any drug, and this is especially true for a bioregulator such as NO. Photochemical uncaging allows one to define the location, timing and dosage of such drug delivery, thus this technique has value as an investigative tool and for addressing the progression of specific disease states.[3–6] In this context, we and others have developed photo-activated NO releasing moieties (photoNORMs), since triggering with light can provide precise spatial and temporal control of NO delivery.[7–10] However, this methodology is limited by the strong wavelength dependence of light transmission through tissue.[11,12] Ultraviolet and shorter visible light are much less tissue penetrating than are longer red or (ideally) near-infrared (NIR) wavelengths. The ability of NIR light to transmit deeply into tissue has inspired various approaches to designing photoNORM systems including the engineering of molecular compounds that are photoactive at longer wavelengths[13,14] and the use of antennas for multi-photon sensitization of NO release with NIR light.[15–18] However, delivering these conjugates to the desired physiological targets continues to be a challenge.

It is difficult to deliver the desired drug payload specifically to hypoxic areas of tumors *via* simple diffusion from the blood stream, owing to poorly developed vascular structures.[19–21] Instead it would be particularly valuable to utilize the inherent biological mechanisms to facilitate such delivery. Tumor hypoxia generates inflammatory signals that recruit monocytes

[a]*Department of Chemistry and Biochemistry, University of California, Santa Barbara, Santa Barbara, CA, 93106 USA. E-mail: ford@chem.ucsb.edu*

[b]*Department of Chemical Engineering, Center for Bioengineering, University of California, Santa Barbara, Santa Barbara, CA, 93106 USA*

[c]*John A. Paulson School of Engineering and Applied Sciences, Harvard University, 29 Oxford St., Cambridge, MA 02138, USA. E-mail: Mitragotri@g.harvard.edu*

[d]*Department of Chemistry and Biochemistry, Doshisha University, 1-3 Tatara Miyakodani, Kyotanabe, Kyoto 610-0394, Japan*

[e]*Molecular Foundry, Lawrence Berkeley National Laboratory, Berkeley, CA, USA*

† Electronic supplementary information (ESI) available: Includes detailed experimental details plus 10 additional figures. See DOI: 10.1039/c8sc00015h

‡ These authors contributed equally to the studies described in this manuscript.

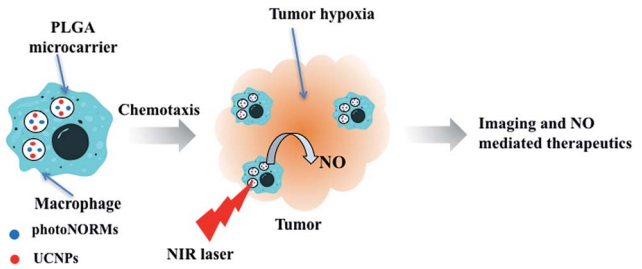

Scheme 1 Illustration of macrophage cellular Trojan Horse strategy to carry polymer based microparticles containing a photochemical precursor of NO (photoNORM) plus upconverting nanoparticles (UCNPs) into a tumor. NIR activation of the photoNORM/UCNP combination releases NO to mediate the tumor environment in order to facilitate various types of therapy as well as providing the opportunity for photoluminescence imaging.

from the blood *via* chemotaxis, that once inside the tumor differentiate into macrophages.[22] This behavior has stimulated interest in recruiting macrophages as carriers[23–28] to localize drugs in tumors at levels difficult to attain with conventional delivery methods.

The present study demonstrates the utility of macrophages as carriers of micron-sized, poly(lactic-*co*-glycolic acid) (PLGA) microparticles in which one can incorporate a theranostic payload. The encapsulated payload here includes a photoNORM that can be triggered for NO release by NIR light together with Nd^{3+} doped upconverting nanoparticles (Nd-UCNPs) to provide imaging capabilities.[29,30] The BALB/c bone marrow derived macrophages (BMMs) were shown to undergo phagocytosis of these microcarriers. Such macrophages allow far deeper penetration into large NIH-3T3/4T1 co-cultured tumor spheroids (Scheme 1) than do the microparticles alone. Thus, as previously described by Clare and coworkers,[23] such macrophages have the potential to act as "cellular Trojan Horses" to carry a therapeutic payload into tumors. It is shown here that, once carried inside the spheroid by a BMM, the photoNORM in the microparticles can be activated with NIR light to release NO. At high light intensity, NO concentrations sufficient to cause direct tumor cell cytotoxicity are generated, while at low light intensity, the NO released leads to a significant drop in the expression of hypoxia inducible factor HIF-1α in the tumor microenvironment.

Results and discussion

NIR active photoNORM and Nd-UCNPs in microparticles

The cell-mediated delivery platform described here consisted of murine BMMs loaded with polymer-based microcarriers into which were incorporated a NIR sensitive photoNORM and NIR active bioimaging Nd-UCNPs. The photoNORM was prepared by metathesis of the water-soluble salt $[Mn(dpaq^{NO_2})(NO)]ClO_4$ ($dpaq^{NO_2}$ = 2-[*N*,*N*-bis(pyridine-2-yl-methyl)]-amino-*N*′-5-nitroquin-olin-8-yl-acetamido)[13] with sodium tetraphenylborate to give the corresponding, hydrophobic photoNORM $[Mn(dpaq^{NO_2})(NO)]BPh_4$ (**I**). The hydrophobicity was needed to minimize leakage of **I** from the polymer microcarrier into the medium. The BPh_4^- salt was further purified by recrystallization to obtain black needles. Fig. 1 (top) shows the spectrum of **I** in acetonitrile. Although the λ_{max} of the longest wavelength band is ~650 nm, this absorbance extends to the NIR region (ε: 20.2 M^{-1} cm^{-1} at 794 nm) and overlaps with the output from a 794 nm diode laser used as a continuous wave (CW) excitation source in the present study. Direct 794 nm photolysis of **I** in acetonitrile solution does indeed lead to NO release as measured using the Sievers Nitric Oxide Analyzer (NOA) with a quantum yield of 0.18 (ESI Fig. S1†).

The Nd-UCNPs were high quality core/shell upconverting nanoparticles (Fig. 1, bottom) synthesized using the robotic Workstation for Automated Nanocrystal Discovery and Analysis (WANDA) of the Molecular Foundry at Lawrence Berkeley National Laboratory.[31–33] The host material for the 10 nm

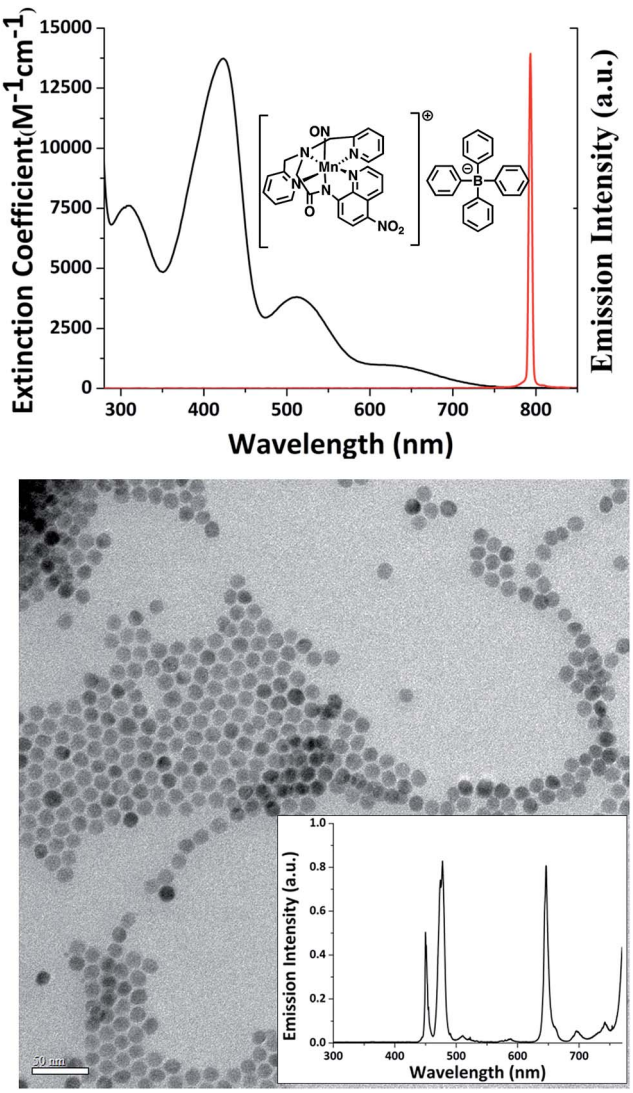

Fig. 1 Top: absorption spectrum of $[Mn(dpaq^{NO_2})(NO)]BPh_4$ (**I**) in acetonitrile. The red spike at the right is the spectrum of the 794 nm diode laser. Bottom: TEM image of the core–shell the nano-particles $NaYF_4$:Yb/Gd/Nd/Tm (30/20/1/0.5%)@$NaGdF_4$:Nd (20%). Inset: upconversion emission spectrum of Nd-UCNPs under excitation by an 800 nm CW laser.

diameter cores was $NaY_{0.8}Gd_{0.2}F_4$. (The Gd^{3+} adduct favors the hexagonal structure that typically gives higher upconversion efficiency).§[34–36] The host material was also doped with the lanthanide ions Yb^{3+} (30%), Nd (1.0%) and Tm (0.5%). The 2 nm thick shell was composed of $NaGdF_4$ doped with Nd^{3+} (20%). The shell minimizes surface quenching effects and improves the luminescence efficiency of UCNPs. The Nd^{3+} sensitizers in these $NaYF_4$:Yb/Gd/Nd/Tm (30/20/1/0.5%)@$NaGdF_4$:Nd (20%) nano-particles (Nd-UCNPs) absorb NIR wavelengths near 800 nm allowing these materials to be excited at wavelengths where the transmittance through water is most efficient. Energy absorbed by Nd^{3+} ions in the shell migrates *via* resonant transfer to Nd^{3+} in the core and energy transfer to Yb^{3+} ions.[36] The energy from multiple photons is transferred sequentially from the excited Yb^{3+} dopants to Tm^{3+} emitters, thereby producing upconverted photoluminescence (PL) bands in the UV and visible range. The transmission electron microcopy (TEM) and PL spectra of these Nd-UCNPs are shown in Fig. 1 (bottom).

The polymer-based microcarriers were prepared from PLGA dissolved in dichloromethane (DCM) by a micro-emulsion technique as described previously[37,38] and in the Experimental methods section (see below). The procedure simultaneously encapsulated the photoNORM **I** and/or Nd-UCNPs into spherical PLGA particles with *ca.* 1-micron diameter (0.35–2 μm) (ESI Fig. S2 & S3†). The average loading of the manganese photoNORM was 4.36 ± 0.66 wt% as determined by inductively coupled plasma atomic emission spectroscopy (ICP-AES). The spherical micro-particles have the optimal shape to facilitate phagocytosis.[39] The PLGA was acid terminated and the resulting surface carboxylates were modified with immunoglobulin G (IgG) by amide coupling in 0.1 M pH 5.5 2-(*N*-morpholino) ethanesulfonic acid (MES) buffer to increase the efficiency of phagocytosis. A bicinchoninic acid (BCA) protein assay indicated there is *ca.* 44 μg of IgG per mg of PLGA particles.

NO release from photoNORM loaded polymer microparticles

Previous studies in these laboratories[16,40] have shown that UCNPs can serve as photosensitizers that absorb NIR photons and emit visible light to trigger NO release from photoNORMs that were not NIR sensitive. This process requires relatively high intensity irradiation to effect the multi-photon upconversion mechanism of UCNPs and energy transfer from UCNPs to photoNORMs. In the present case, the Mn photoNORM **I** is photosensitive toward NO release *via* direct single-photon excitation with 794 nm light, and this allows one to overcome the scattering constraints that may be problematic for multi-photon excitation in deeper tissue. However, since the extinction coefficient for **I** at this wavelength is low (20.2 M^{-1} cm^{-1}), it was of interest to see whether the visible light generated by upconversion from the Nd-UCNP would enhance NO release owing to the significantly higher extinction coefficients of **I** in the visible spectral region.

In order to test this possibility, microparticles of two different compositions were prepared. One contained both **I** and Nd-UCNPs (PLGA-1), the other contained only the manganese photoNORM **I** (PLGA-2). Data obtained from dynamic light scattering (DLS) showed these two particle groups to be similar in average size (~1 micron, ESI Fig. S2† top), while ICP-AES analysis showed the former to have somewhat higher loading of **I** (4.76 wt% *vs.* 3.79 wt% respectively). Particles of both types (0.5 mg) were separately suspended in 2.5 mL pH 7.4 phosphate buffered saline (PBS) solution and were irradiated with a 794 nm diode laser while stirring and purging with medical grade air. The purge gas was analyzed for NO using the NOA for 1.0 s irradiation times at different intensities (in W cm^{-2}). The NOA signals recorded are shown in ESI Fig. S3† while Fig. 2 plots the quantity of NO released from these microcarriers in response to the different excitation laser intensities. Notably, both plots appear roughly linear over this narrow range, consistent with a single photon excitation mechanism for NO release. Additionally, the efficiencies of NO release for PLGA-1 and PLGA-2 are 1.63 pmol W^{-1} cm^2 s^{-1} and 2.06 pmol W^{-1} cm^2 s^{-1} respectively. When differences in loading are taken into account, this represents a lower NO release from the Nd-UCNP loaded microparticles, although this experiment is somewhat qualitative given that these are suspensions of the microparticles. Nonetheless, under these experimental conditions, the Nd-UCNPs have value primarily for imaging purposes.

Microparticle uptake and compatibility

The goal of these experiments was to determine the amount of loaded PLGA microparticles that can undergo phagocytosis into the murine bone marrow macrophages that had been prepared as described in the Experimental section (see ESI†). It has been previously shown that rigid spheres, 1–3 microns in diameter, are readily taken up by this mechanism.[27,41,42] As noted above, said microparticles were also surface modified with a covalently bound layer of IgG to enhance uptake (ESI Fig. S4†). An alamarBlue® cell viability assay was used to determine whether

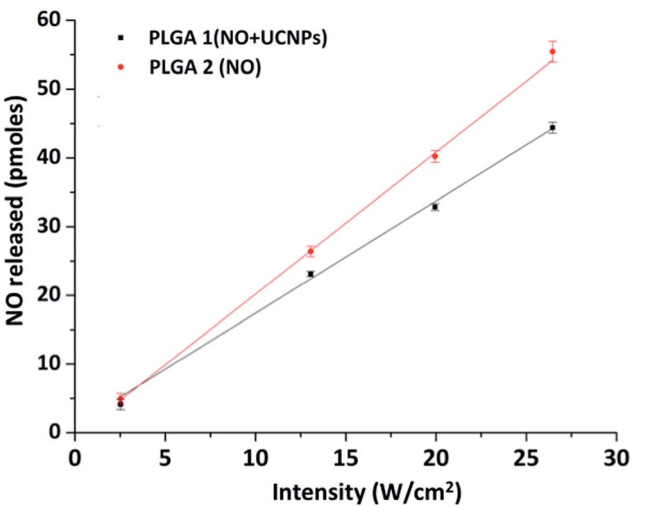

Fig. 2 Plots of the NOA detected NO released *vs.* laser intensity (W cm^{-2}) for the CW 794 nm photolysis of PBS suspensions of the microcarriers PLGA-1 (black) and PLGA-2 (red).

the microparticles proved toxic to the BMM cells. Fig. 3 shows that these particles displayed no significant acute toxicity for concentrations as high as 100 μg mL^{-1} for incubation periods of 24 and 48 h with BMMs. Moderate toxicity was observed at higher concentrations. (Notably, a recent review of lanthanide-UCNP toxicity has stated that, while there are numerous reports of negligible or low toxicity, "there is a paucity of knowledge concerning primary and secondary toxicity effects on the environment and humans.")[43] For the present study, the microparticle concentration of 100 μg mL^{-1} was selected for further incubations. Analysis of BMMs containing NO-donor loaded particles with ICP-AES determined an uptake of 0.667 μg manganese per 1×10^6 cells. This translates into 263 μg particles or 12.1 nano-equivalents of NO as photoNORM **I** in 10^6 cells.

Intracellular NO release

BMMs loaded with microparticles containing both **I** and Nd-UCNPs ($BMMp^+$) were then tested to verify internal release of NO. The reporter was 4-amino-5-methylamino-2′,7′-difluorofluorescein diacetate (DAF-FM), which reacts to form a fluorescent compound when exposed to intracellular NO. DAF-FM was incubated with the $BMMp^+$ macrophages and a control set of BMMs without microparticles. Prior to DAF-FM incubation, both sets were treated with L-*N*-nitroarginine methyl ester (L-NAME), a nitric oxide synthase inhibitor, to reduce background from biological NO production.[44] Upon 794 nm laser exposure at 13.0 W cm^{-2} for 90 s, the $BMMp^+$ set clearly produced a visible fluorescence response while the BMM set without particles did not (ESI Fig. S5†).

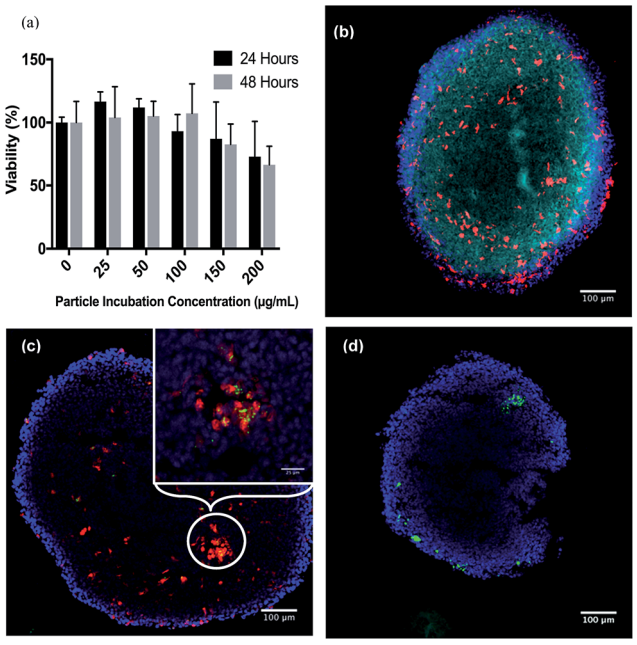

Fig. 3 (a) Viability of BMMs with various particle incubation concentrations after 24 and 48 h. (b)–(d) Are slices of 4T1/NIH-3T3 co-cultured breast tumor spheroids imaged by confocal microscopy. Blue is 4′,6-diamidino-2-phenylindole (DAPI) and red represents macrophages stained with CellTracker™ deep red. Green spots in (c) and (d) are Cy-3–IgG labeled microparticles. (b) Spheroids stained with a Hypoxyprobe™ Red549 to label hypoxia (cyan). (c) Spheroid incubated with microparticles-laden BMMs. (d) Spheroid incubated only with IgG modified PLGA microparticles.

Microparticle effects on macrophage chemotaxis

The ability of macrophages to target tissue such as tumors is governed by their ability to undergo chemotaxis towards sites of inflammation.[22] Thus, it is crucial that the macrophages retain this function after drug loading. This question was probed using a transendothelial assay (ESI Fig. S6†). First, monolayers of bEnd.3 blood brain barrier (BBB) endothelial cells were grown on FluoroBlok™ transwell inserts inside of the wells of a 24-well plate as model endothelium barriers. Such monolayers are very tight compared to those from other endothelial cells, thereby making migration through the barrier challenging.[45]

After monolayer confluency, media containing 1×10^5 $BMMp^+$ cells, media containing a comparable number of BMMs without particles, and media alone were added to the tops of separate transwells and the monocyte chemoattractant protein-1 (MCP-1) was added below. After 24 h, the inserts were stained with NucBlue® allowing for quantification of chemotaxis by counting the nuclei of cells that had migrated to the bottom of the insert using a fluorescence microscope (corrected for the signal from wells with a confluent monolayer to which only media had been added). This analysis showed migration of both the native BMM cells and the $BMMp^+$ cells across the endothelium layers, although under these conditions, fewer of the $BMMp^+$ cells ($(10.4 \pm 0.8) \times 10^3$) migrated relative to the BMM control cells ($(17.1 \pm 2.4) \times 10^3$). Thus, phagocytosis of microparticles did reduce chemotaxis as reported previously,[27] although in the latter case an even sharper drop in chemotaxis was observed. However, there are various strategies that can be used to enhance overall macrophage recruitment and therapeutic efficacy, if needed.[28,46,47]

Tumor spheroid penetration

In order to model a 3D tumor environment, tumor spheroids were prepared from co-cultured murine NIH/3T3 fibroblast: 4T1 breast cancer cells with a 5 : 1 cell seeding ratio similar to that used previously.[48] Incorporation of fibroblasts into tumor spheroids induces formation of a tumor stroma which enhances spheroid compactness and increases the expression of pro-inflammatory cytokines used in leukocyte chemotaxis.[49] With this seeding ratio, the hanging drop technique produced spheroids with an average diameter of 962 ± 60 μm (~1.35×10^5 cells per spheroid) after 10 days of incubation with the microparticle loaded macrophages introduced on day 7. These spheroids are considerably larger than those produced with 4T1 cells alone (ESI Fig. S7†) as well as those NIH/3T3: 4T1 spheroids grown without the loaded BMM cells (ESI Fig. S8†), the latter a likely result of macrophage supported tumor growth.[49] Pimonidazole (PIMO) staining of the spheroids revealed hypoxia throughout the spheroid interior. Considering that hypoxia normally occurs 100–150 μm into a tumor,[50] this is not surprising.

Macrophages labeled with Celltracker™ deep red were used to monitor the chemotactic penetration of the $BMMp^+$ cells into spheroids. Images of tumor spheroid center slices indicated deep penetration (Fig. 3b), although the macrophages did not reach the center but instead formed a visible ring around the central section. Since oxygen is required for macrophage chemotaxis, this behavior may reflect a central necrotic region with high hypoxia. Flow cytometry of spheroids dissociated with Accumax™ demonstrated a macrophage cell composition of $0.53 \pm 0.4\%$ or $\sim 715 \pm 540$ macrophages per spheroid (ESI Fig. S9†). Assuming that the $BMMp^+$ retained their payload at the concentration shown by ICP, these macrophages brought an estimated 8.7 ± 6.6 pico-equivalents of the photoNORM into the spheroid. The value of the macrophages as "Trojan Horses" was demonstrated using particles labeled with fluorescent IgG. Spheroid slices (Fig. 3c) demonstrated that macrophages with internalized fluorescent particles carried their payload into the spheroids (Fig. 3c) but that IgG modified microparticles alone were unable to penetrate more than a few cell layers when incubated with the spheroids (Fig. 3d).

Nd-UCNP imaging

The Nd-UCNPs introduced to the polymer-based microparticles provide an imaging agent that allows one to track the location of these prodrug carriers and their macrophage hosts using tissue-penetrating NIR excitation wavelengths. In addition, since their chemotactic capacities allow macrophages to hone in on inflammation sites, the PL from UCNPs provides a potential mechanism to detect hidden metastatic sites. Since **I** is photoactivated by the same NIR wavelength, the combination of this photoNORM and Nd-UCNP in these macrophage-carried microparticles would provide theranostic capability.

Fig. 4 shows 3D images of spheroids incubated with $BMMp^+$ or with $BMMp^-$ and recorded with a confocal microscope using a 808 nm laser source. The spheroids were labeled with calcein AM to provide visualization of their periphery. PL signals were noted from the spheroids treated with $BMMp^+$ cells while those treated with $BMMp^-$ cells failed to produce a signal. These luminescent emissions from the Nd-UCNPs provide a proof-of-principle with regard to using UCNPs to track the macrophages, but it is clear that either more efficient emitters or (given that the nonlinear relationship between UCNP PL and excitation intensities) a more intense laser source may be needed for *in vivo* diagnostic applications. On-going studies will address this issue.

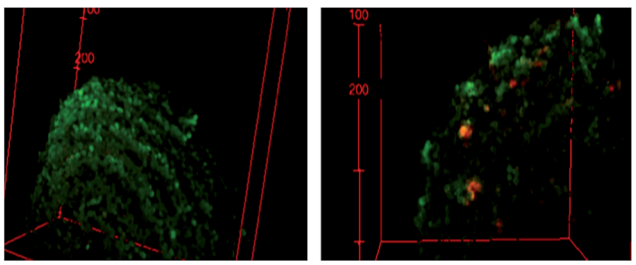

Fig. 4 Z-stack two-photon confocal images (dimensions = 508.4 μm × 508.4 μm) of live spheroids containing BMMs (left) with blank particles and (right) with UCNP and NO-donor loaded particles. Spheroids were stained with calcein AM (green). Particles were identified *via* emission (red) from embedded UCNPs with laser excitation at 810 nm and a pulse energy of 37.5 nJ. The wavelength range for detection of UCNP emission was 420–460 nm.

Photoactivated NO release inside spheroids

The next question was whether NO released by NIR excitation of these $BMMp^+$ infiltrated spheroids can be detected externally using the NOA, which to the best of our knowledge, would be unprecedented. Five spheroids incubated with $BMMp^+$ or BMMs with PLGA-only particles ($BMMp^-$) were positioned in the corner of a custom designed cuvette (Fig. 5a) containing 1 mL of Hank's Balanced Salt Solution (HBSS) solution. In typical NOA analysis, the solution is entrained with the carrier gas and stirred to facilitate transfer of NO to the detector. However, such conditions would likely cause spheroid disassembly and cell lysis. Instead, the spheroids were blanketed with unstirred HBSS solution and irradiated with the 794 nm diode laser operating at 13.1 W cm^{-2} for specified time periods (Fig. 5a). Subsequent gentle bubbling with medical-grade air above the spheroids released NO from the solution without disrupting the spheroids. The procedure could be repeated

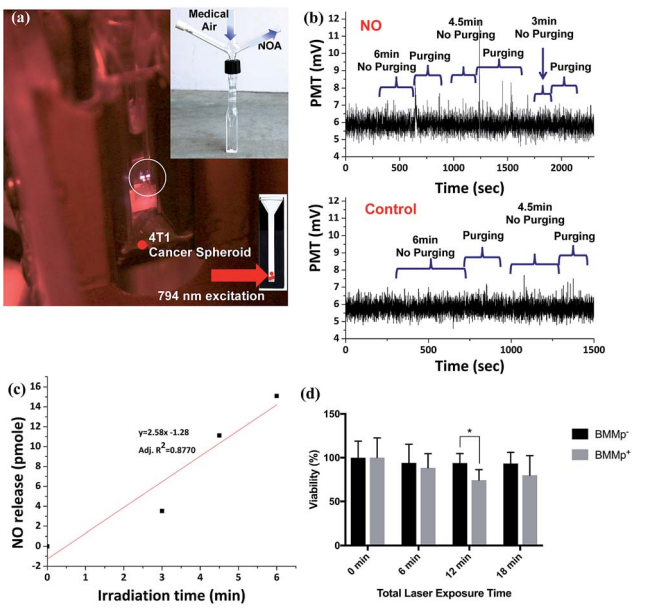

Fig. 5 (a) The NIH/3T3:4T1 tumor spheroids in 1 mL Hank's buffered salt solution (HBSS) under 794 nm laser irradiation (photo by Ping-Lin Yang). Inset (up): a modified 1 mL cuvette for photolysis experiment of cancer spheroids. Inset (down): the scheme represents that the spheroids can be placed at the corner of the cuvette and exposed to NIR laser excitation. (b) Up: NO released from five spheroids infiltrated with bone marrow macrophages loaded with PLGA microparticles containing **I** and Nd-UCNPs under 794 nm laser irradiation with 13.1 W cm^{-2}. Down: the control experiment of six spheroids loaded with PLGA microparticles. (c) Plot of NO detected *vs.* irradiation time. (d) The viability of spheroids after 6, 12, or 18 min of laser exposure in 6 min increments. Viability was measured using a PNPP assay 24 h after spheroid treatment. $*p \leq 0.05$ (Students *t*-test).

several times with each sample (Fig. 5b and c). The NO released photolysis from the five $BMMp^+$ infiltrated spheroids after the 6 min (total) was 13.6 pmol (~2.7 pmol per spheroid (avg)). In contrast, spheroids treated with $BMMp^-$ cells gave no measurable NOA response. Based on volumes of ~1 μL, NO steady state concentrations in excess of 1 μM were generated in the spheroids, a concentration exceeding that needed to induce p53 phosphorylation and/or nitrosative stress mediated apoptosis.[1]

The effect of generating such high localized NO concentrations was examined by evaluating cell viability after 24 h using a *p*-nitrophenyl phosphate (PNPP) assay.[51] Fig. 5d illustrates the results of irradiating spheroids containing $BMMp^+$ or $BMMp^-$ cells with 794 nm light for 1 to 3 six-minute periods at 13.1 W cm^{-2}. In general, the data in Fig. 5d consistently show reduced cell viability for irradiated spheroids infiltrated with $BMMp^+$ cells relative to those loaded with $BMMP^-$ cells, the most convincing example being the 26% reduction for spheroids containing photoNORM loaded macrophages after 12 min irradiation compared to 6.6% reduction for similarly treated $BMMp^-$ loaded spheroids. However, the experimental uncertainties are large and barely statistically significant owing no doubt to unavoidable variability in spheroid loadings and the difficulty in preparing, photolyzing and analyzing a statistically large number of loaded spheroids. Notably, the spheroids used in this study were formed from 4T1 breast cancer cells, which are p53 deficient,[52] so the observed damage can largely be attributed to nitrosative stress induced apoptosis. Cancers with p53 pathways are likely to be more sensitive to NO delivery at these concentrations.

Low NO concentrations have been shown to produce beneficial shifts in tumor microenvironment through reduction of factors such as *P*-glycoprotein and HIF-1α that are implicated in increased resistance to chemo- and radio-therapy.[53–55] HIF-1α is a transcriptional factor upregulated in hypoxia that controls the expression of genes correlated with tumor cell survival, metastasis, and angiogenesis.[56] The effect of generating lower NO concentrations on HIF-1α levels in the tumor spheroids was examined by using LED excitation (0.58 mW cm^{-2} at 735 nm). After 8.5 h exposure, the spheroids were dissociated into a single cell suspension. Cells were then fixed and labeled with anti-HIF-1α and by a fluorescent secondary antibody. Analysis with flow cytometry (Fig. 6) revealed that the low intensity excitation at 735 nm reduced proportion of cells expressing HIF-1α from 96.7 ± 0.5% to 77.7 ± 8.7% in irradiated spheroids containing $BMMp^+$ macrophages while spheroids with infiltrated with $BMMp^-$ macrophages showed little change in HIF-1α level upon excitation. These data agree with previous studies demonstrating that low concentrations of NO destabilize HIF-1α in hypoxia due to the inhibition of cytochrome c oxidase,[54] a critical component of mitochondrial respiration. In a second trial, HIF-1α expression in spheroids containing $BMMp^-$ and $BMMp^+$ macrophages was shown by flow cytometry to be 90.3 ± 5.1% and 62.2 ± 2.5%, respectively, after LED excitation for 7 h (ESI Fig. S10†), thus confirming the impact on this proliferative factor upon delivering a low concentration of NO.

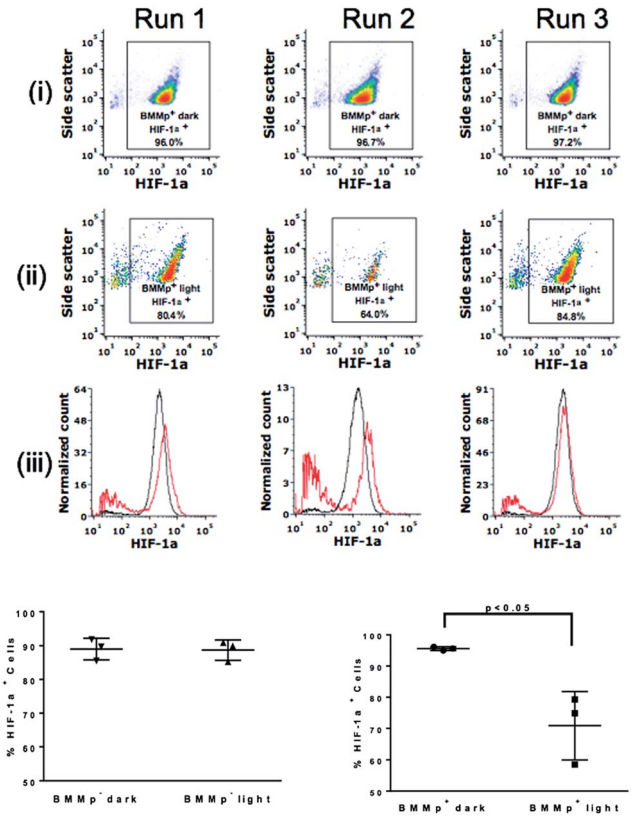

Fig. 6 Top: flow cytometry analysis of dissociated tumor spheroids stained for HIF-1α under different treatments. Gated cells correlate with a positive signal from staining. (i) and (ii) Three runs of analysis for spheroids loaded with PLGA microparticles incorporating I and Nd-UCNPs with and without 735 nm LED irradiation at 0.58 mW cm^{-2} for 8.5 h. (iii) The comparison of (i) and (ii) for each run. Red and black lines represent particles with and without light irradiation respectively. Bottom: the summary of flow cytometry analysis for the control (i) and the NO release study (ii).

Summary

These studies demonstrate that the timing and dosage of NO release from photoNORM loaded microparticles can be controlled inside tumor models by triggering with tissue penetrating NIR light. Bone marrow derived macrophages serve as Trojan Horse carriers for the polymer-based microparticles incorporating both the photoNORM (**I**) and Nd^{3+}-doped upconverting nanoparticles for therapeutic and imaging applications. In this manner, the carrier macrophages load large quantities of a photoactivated therapeutic agent without significant effects on viability. The loaded $BMMp^+$ cells maintain the chemotactic ability to traverse an *in vitro* brain blood barrier transendothelial model and to penetrate tumor spheroids with their photoactive cargos. Such penetration does not occur with the microparticles alone. However, while the tumor spheroids provide a valuable proof-of-principle, *in vitro* model to demonstrate that macrophages can infiltrate and deliver a payload to such tissues, the next stage will be to demonstrate such targeting *in vivo*. In this context we are encouraged by a recent study[57] where blood monocytes loaded with nano-sized

polymeric micelles containing paclitaxel (PTX) were used to treat metastatic breast cancer in mice. Such PTX delivery was significantly more efficient than using free PTX or PTX loaded nanoparticles alone.

Both **I** and the Nd-UCNPs are excited with NIR light at ~800 nm, the ideal wavelength for tissue transmission. Thus, the Nd-UCNP emission is used to visualize $BMMp^+$ cells infiltrated into spheroids while NIR photoactivation of **I** released NO. We demonstrate two types of potentially therapeutic effects by using different light intensities to irradiate the $BMMp^+$ cell infiltrated tumor spheroids. The micromolar NO concentration generated by high intensity NIR laser excitation leads to increased nitrosative stress and cell mortality. In contrast, lower concentrations of NO served to modify the tumor microenvironment by destabilizing HIF-1α. Although not explored in the current study, it should be noted that targeted NO release in the hypoxic regions of tumors should enhance the effectiveness of cancer chemotherapy[55] and radiotherapy.[58,59] In these contexts, macrophage-mediated delivery of photoNORMs combined with NIR excitation represents a fresh approach that allows one to target tumors or other diseased tissues characterized by inflammation. This strategy will facilitate the spatially and temporally controlled release of NO or of other caged compounds for precise therapeutic applications.

Experimental section

Materials

All cell lines (4T1, NIH-3T3, and bEnd.3) were purchased from ATCC. BALB/c mice (6–8 weeks old) were purchased from Charles River. Sodium tetraphenylborate, sodium trifluoroacetate, sodium oleate, ammonium fluoride, lanthanide chlorides (99.9+%), oleic acid (OA) (90%), 1-octadecene (ODE) (90%), poly(vinyl) alcohol (PVA, M_w: 13 000–23 000), 4-morpholineethanesulfonic acid (MES, low moisture content, 99+%), immunoglobulin G (IgG from mouse serum), *N*-(3-dimethylaminopropyl)-*N*′-ethylcarbodiimide hydrochloride (EDC·HCl, commercial grade), Triton™ X-100 (BioXtra), Tween® 20 (BioXtra), agarose (BioReagent), sodium hydroxide (NaOH, ACS reagent grade), sodium acetate (RegentPlus®), purified human plasma fibronectin (1 mg mL^{-1}), and Perfecta3D® 96-well hanging drop plates were purchased from Sigma-Aldrich. 10× PBS (OmniPur® liquid concentrate) was purchased from EMD Millipore. Poly(lactic-*co*-glycolic acid) (5050 DLG 8A, acid terminated) was purchased from Lakeshore Biomaterials. 4-Amino-5-methylamino-2′,7′-difluorofluorescein diacetate (DAF-FM-2DA, Molecular Probes®) was purchased from Life Technologies. *N*-Hydroxysuccinimide (NHS), fetal bovine serum (FBS), Dulbecco's Modified Eagle Medium high glucose (DMEM), Dulbecco's Modified Eagle Medium: Nutrient mixture F12 GlutaMAX™ and high glucose (DMEM/F12), sodium pyruvate solution (100 mM), penicillin streptomycin 10 000 U mL^{-1} (P/S), trypsin/EDTA (0.25%), Hank's Balanced Salt Solution without calcium and magnesium (HBSS), Dulbecco's Phosphate Buffered Saline without calcium and magnesium (DPBS), NucBlue®, CellTracker™ deep red, goat serum, FITC labeled goat-anti-rabbit, rabbit anti-HIF-1α, *p*-nitrophenyl phosphate (PNPP) substrate tablets, calcein AM, micro bicinchoninic acid assay kit, and alamarBlue® was purchased from Thermo Fisher Scientific. All TC and Non-TC treated plasticware for cell culture, and Fluoroblok™ transwell inserts were purchased from Corning. Bambanker™ cell freezing media was purchased from Bulldog Bio. Accumax™ was purchased from Innovative Cell Technologies. L-*N*-Nitroarginine methyl ester hydrochloride salt (L-NAME) was purchased from Caymen Chemical. Murine monocyte colony stimulating factor 1 (MCSF-1) and murine monocyte chemoattractant protein 1 (MCP-1) were purchased from Peprotech. Hypoxyprobe-Red549 Kit containing pimonidazole HCl and mouse Dylight™ 549-Mab was purchased from Hypoxyprobe. Immunoglobulin G labeled with Cyanine 3.5 (Cy3.5–IgG) was purchased from Jackson Immuno.

The $[Mn(dpaq^{NO_2})(NO)]BPh_4$ salt (**I**) was prepared under reduced lighting by anion metathesis of the perchlorate analog that had been synthesized as reported.[13] $[Mn(dpaq^{NO_2})(NO)]ClO_4$, (119.3 mg, 0.195 mmol) was dissolved in 3 mL solution of 1 : 1 acetonitrile/deionized (DI) water that was then added to a 2 mL volume of acetonitrile (ACN) in which was dissolved $NaBPh_4$ (66.7 mg, 0.195 mmol). The resulting mixture was sonicated for 3 min after which most of the solvent was removed under reduced pressure. The resulting hydrophobic black solid was suspended in aqueous solution then collected by filtration, washed with DI water and dried under vacuum. The solid was then dissolved in dichloromethane (DCM) and recrystallized by vapor diffusion of ether to produce crystalline black needles of **I**.

IgG-modified microcarriers

The procedure for forming the polymer micro-emulsions was modified from the literature.[37–39] Acid-terminated PLGA (100 mg) and ~80 μL of a solution of Nd-UCNPs in hexane (~10 mg UCNPs) were added into 500 μL DCM, and the mixture was sonicated for 45 min at room temperature. A 14 mg sample of **I** was dissolved in a mixture of ACN (150 μL) and DCM (400 μL) to form a dark purple solution that was then transferred into the PLGA solution, and the mixture was sonicated until homogenous. If the volume of as-prepared solution was lower than 1.1 mL, more DCM was added. The polymer solution was slowly added into 200 mL of 1 wt% polyvinyl alcohol (PVA) aqueous solution contained in a 250 mL half-spherical container while the ultrasonic homogenizer was turned to 350 watts for 30 s. A dark brown colloidal solution formed immediately. The flask containing the colloidal suspension was fully covered with aluminum foil and stirred overnight to evaporate the volatile organic solvents. The milky solution was centrifuged to collect a solid, which was washed with 18 megohm pure water to remove the PVA. Following particle purification, the brown pellet was re-suspended in 45 mL pure water and then the 1-micron particles were separated by different centrifuge speed (4000 rpm to remove particles <500 nm and 300 rpm to remove particles size >3 μm). The resulting particles were dried under vacuum and re-suspended in 0.1 M pH 5.5 MES buffer solution with the concentration of 1 mg mL^{-1}. EDC·HCl (70.94 μmol per 1 mg particles) and NHS (106.87 μmol per 1 mg particles) were added into the colloidal MES solution, which was then

sonicated at room temperature for 30 min. Subsequently, 10 μL IgG solution (11.21 mg mL^{-1}) per 1 mg microparticles was added and the mixture stirred overnight. The IgG modified particles were collected by centrifugation and washed with 18 megohm pure water at least three times. IgG concentration was determined with a micro BCA assay according to the manufacturer's instructions. After incubation, particles were removed from solution with centrifugation to avoid light scattering during absorbance measurements.

Initially, a beaker was utilized during the emulsion process, however; better yields were obtained using a half-spherical glass flash, since there are no corners in the latter and the sonic energy is distributed equally preventing settling and allowing more of the PLGA to form particles of the correct size.

Bone marrow macrophage preparation and other cell cultures

Bone marrow was harvested from 6–8 week old BALB/c mice in accordance with previously published methods.[60] Experiments were performed in compliance with all United States federal and California state regulations governing the humane care and use of laboratory animals, including the USDA Animal Welfare Act (Registration #: 93-R-0438) and the PHS Policy on Humane Care and Use of Laboratory Animals (PHS Assurance # A3865-01) and were reviewed and approved by the University of California Santa Barbara Institutional Animal Care and Use Committee as part of protocol 6-16-916. After marrow isolation, cells were then suspended in a 90% FBS/10% dimethyl sulfoxide (DMSO) and frozen for later use according to previous reports.[61]

Unless otherwise specified, all culture ware used with macrophages was non-TC treated plastic. Bone marrow macrophages were produced *via* slight modification of previously published methods.[60] Cryo-preserved bone marrow was thawed and added to 10 mL of DMEM/F-12 media supplemented with 10 mM GlutaMAX™, 10% FBS, 1000 U mL^{-1} P/S, and 20 ng mL^{-1} MCSF-1 (media denoted as DMEMb) cells were centrifuged at 400 g for 10 min, resuspended in DMEMb at 2.3×10^6 live cells per mL. DMEMb (24 mL) and 1 mL of bone marrow were added to a flask and put in the incubator for 7–8 days to allow the bone marrow to mature into BMMs. On day 3, 25 mL of additional DMEMb was added to each flask to replenish the MCSF-1 in solution. After cells had matured into BMMs, DMEMb was removed from the flask and cells were washed with DPBS. To dislodge the cells, the flask was treated with ice cold Accumax™ (10–15 mL) for 20–30 min, and thumped once with the palm of the hand. Cells were collected, washed with DMEMb and centrifuged at 400 g for 10 min. Cells were resuspended in Bambanker™ cell cryopreservation media at 5×10^6 cells per mL. BMMs were kept at −80 °C overnight and were transferred to liquid nitrogen afterwards. Confirmation of macrophage maturation was done using CD11b staining as described by Zhang *et al.*[60]

For experiments, BMMs were thawed and added to non-TC treated dishes for 24 h. Cells were then detached with Accumax™ and counted. These cells were then replated at 62 500 BMM per cm^2 on plastic ware 18 h prior to the experiment.

NIH-3T3 murine fibroblast cells, 4T1 murine breast cancer cells, and bEnd.3 murine brain endothelial cells between passage 3–15 were cultured on TC-treated plastic ware with Dulbecco's modified eagle medium (DMEM) supplemented with 10% fetal bovine serum (FBS), 1000 U mL^{-1} of penicillin/streptomycin (P/S) and 1 mM sodium pyruvate (media mixture known as DMEMpy). Cells were passaged with 0.25% trypsin/EDTA once they reached a confluency of >80%.

Tumor spheroids

Tumor spheroids were grown with a procedure based on previous research.[48] Confluent plates of 4T1 and NIH-3T3 cells were split and resuspended in DMEMpy and then mixed at a ratio of 1 : 5 4T1 : NIH-3T3 at a total cell concentration of 1.11×10^4 cells per mL. To prevent evaporation of the hanging drops, the liquid reservoirs on 96 well hanging drop plates from 3d Biomatrix were filled with hot 0.5% w/v agarose and allowed to cool to room temperature. A 45 μL aliquot of the cell mixture was added to the top of each well. Plates were sealed with Parafilm® and put in the cell incubator for 7 days. Media was replenished on days 4 and 6 by removing 15 μL of media from each droplet and adding 15 μL of fresh DMEMpy. This procedure was done 2 times in a row during each media change instead of removing 30 μL of media all at once which can compromise the droplet. Spheroids were grown in droplets for 7 days.

To incorporate macrophages, spheroids were transferred into 200 μL 96 well PCR plates used to allow for their easy manipulation and inversion on the rotisserie without spilling. Spheroids were washed 3 times with 100 μL of DMEMpy. DMEMpy (50 μL) was added to each spheroid after the final wash. A 50 μL aliquot of a solution of BMMs with blank or NO-donor loaded particles at 4×10^5 cells per mL in DMEMpy was added to each spheroid. Plates were put on a rotisserie in a cell incubator for 3 days to assure optimal interaction between macrophages and spheroids. On day 1.5, 100 μL of additional DMEMpy was added to each spheroid to replenish solution nutrients. After 3 days, spheroids were washed 3 times with DMEMpy to remove macrophages that had failed to infiltrate the spheroid. Spheroids were then used for various downstream applications.

Particle loading into BMMs

Particles with or without NO-donor and UCNPs in DI water at a concentration of 5 mg mL^{-1} in a glass vial were sonicated for 10 min to break up particle aggregates. A volume of 340 μL of the microparticle solution was added to macrophages plated at 62 500 cells per cm^2 in a 100 mm diameter non-TC treated Petri dish in 17 mL of DMEMb to make a 100 μg mL^{-1} solution. Dishes were put in a culture incubator for 2 h to allow for phagocytosis. Cells were washed once with warm DPBS after which, ice cold Accumax™ (5 mL) was added and incubated at 37 °C for 15–30 min. Cells were then pipetted up and down gently to release them from the plate. DMEMb (5–7 mL) was added to the cell suspension. Cells were centrifuged once at 400 g for 10 min and resuspended in 2 mL DMEMb. Cells were then centrifuged 3 times at 42 g for 5 min to remove free particles in solution. In cases where macrophage tracking was

desired, 2 μM CellTracker™ deep red in serum free DMEMb was added to cells for 45 min before Accumax™ was applied.

Quantification of particle loading and macrophage uptake

Particles of a known concentration containing the NO-donor and UCNPs were digested in 1 : 3 HNO_3 : HCl for 24 h to assure all manganese was completely dissolved. Inductively coupled plasma atomic emission spectroscopy (ICP-AES) was conducted with a Thermo iCAP 6300 and was used to measure the manganese content of each sample. Samples were compared to manganese standard. For quantification of particle uptake, 3×10^6 cells with particles were analyzed in the same manner. These cells were compared to cells without particles.

Macrophage-particle compatibility

Macrophages loaded with microparticles as described above with various particle incubation concentrations were plated at 62 500 cells per cm^2 in 96 well plates in 100 μL DMEMb. Cells were put in a cell incubator and left for 24 or 48 h. A mixture containing 100 μL of DMEMb and 20 μL of alamarBlue® was added to the media in each well. The plate was incubated for 3.5 h. A volume of 110 μL of each well was transferred to black bottomed well plates to improve the sensitivity of the fluorescence measurement. Solution fluorescence was measured on a TECAN M220 Infinite Pro plate reader (λ_{ex} = 550 nm, λ_{em} = 590 nm). Fluorescence from wells without cells was subtracted as baseline.

Qualitative determination of NO release

Human fibronectin at 150 μg mL^{-1} in DPBS was added to glass confocal dishes and incubated for 2 h at 37 °C to improve its cell adhesion properties. Wells were washed 3 times with DPBS. Macrophages with particles were plated in the glass confocal dishes at 62 500 cells per cm^2 and incubated for 8 h in DMEMpy. Cells were incubated with L-NAME at 75 μg mL^{-1} in DMEMpy for 1 h to inhibit biological NO production from nitric oxide synthases. Wells were aspirated and 9.3 μM 4-amino-5-methylamino-2′,7′-difluoroflurescein (DAF-FM-2DA), a dye that detects intracellular NO release, with L-NAME in DMEMpy was added to the cells and incubated for 1 h. Wells were washed five times with phenol red free, FBS free DMEMpy with L-NAME to remove uninternalized DAF-FM. Wells were exposed to a 794 nm laser for 90 s at 13.1 W cm^{-2}. NucBlue® was added to the wells to label cell nuclei. Wells were imaged 20 min later. Images were taken with an Olympus Fluoview 1000 Spectral Confocal. Care was taken to image cells as quickly as possible to prevent the release of extra NO. Samples were compared to macrophages exposed to the laser without particles.

Quantification of macrophage chemotaxis

Human fibronectin (50 μL, 150 μg mL^{-1}) in DPBS was added to the top of 24-well sized FluoroBlok™ transwell inserts with 8 μm pores and incubated in a cell incubator for 1.5–2 h to improve their adhesion properties for endothelial cells. The top of the inserts was washed 3 times with 200 μL of DMEMpy. A 200 μL aliquot of bEnd.3 cells at a concentration of 1×10^5 cells per mL were added to the top of each well. Cells were incubated for 4.5 days with media changes every other day. No media was added to the bottom of the insert until the final day to prevent the growth of a monolayer in the bottom of the insert which has been reported previously when media is added to both sides.[62] On day 4.5, media in the top insert was replaced and 600 μL of DMEMpy was added to the bottom of the insert. Transepithelial electrical resistance (TEER) values were taken and all inserts with a value ≥0.33 Ω cm^2, which traditionally represents a fully confluent monolayer, were accepted for the experiment. Inserts were washed 3 times with DMEMpy. 200 μL of either DMEMpy alone, or BMMs with or without particles at 5×10^5 cells per mL in DMEMpy were added to the top of the inserts and 600 μL of DMEMpy with 125 ng mL^{-1} MCP-1 was added to the bottom of each well to serve as a chemoattractant for the macrophages. Cells were incubated for 24 h in a cell incubator and washed once with DPBS. NucBlue® in HBSS was added to the top and bottom of each insert to visualize cells. After 20 min, images from 3 random locations from the bottom of each insert were taken with an Olympus CKX-41 inverted microscope. Cells were counted with the particle analysis tool on ImageJ. Wells that contained only a bEnd.3 monolayer were used as a baseline and were subtracted out of macrophage wells.

Determination of macrophage/spheroid penetration

Macrophages labeled with CellTracker™ deep red were allowed to penetrate spheroids as described above to allow for visualization. Spheroids were fixed in ice-cold methanol for 30 min. Spheroids were then embedded in Tissue-Tek® O. C. T. compound and sectioned with a 25 μm thickness. Spheroids were mounted with Vectashield® hard set mounting media with 4,6-diamidino-2-phenylindole (DAPI) to preserve samples and stain cell nuclei. For hypoxia detection, some spheroids were incubated with 100 μM PIMO in DMEMpy for 2 h prior to fixation with methanol (MeOH). This allowed PIMO to fully infiltrate spheroids and covalently bind to cells in hypoxic regions. After sectioning, these samples were blocked with PBS containing 4% FBS, 1% goat serum, and 0.05% Tween® 20 (blocking solution) for 1 h. Hypoxyprobe Red549 (#HP7-100Kit; Hypoxyprobe) in a 1 : 200 dilution in blocking solution was added to each spheroid for 18 h at 4 °C to allow the antibody to bind to the PIMO present in the sectioned spheroid. Sections were then washed three times with PBS with 0.05% Tween® 20. In other experiments to demonstrate retention of particles after spheroid penetration, particles were labeled with Cy3.5®–IgG. Because of the overlap between Hypoxyprobe Red549 and Cy3.5®, they were not used together. Images were acquired with an Olympus Fluoview 1000 spectral confocal microscope and processed with ImageJ.

NO release measurement

The NO measurement followed the modified procedure from the literature.[16] All spheroids were carefully transferred to 1 mL HBSS solution in a modified cuvette and closely placed at the corner in order to get full exposure with a 794 nm diode laser.

Medical-grade air was purged into the cuvette through plastic tubing but not directly purged into the solution. Laser intensity 13.1 W cm^{-2} was applied to all spheroid-involved measurement. During the period of laser irradiation on these spheroids, the medical air purging was only above the solution. But once the irradiation was stopped, the purging tubing was manually immersed into the solution carefully in order to avoid agitating these spheroids. The flowing gas conveyed the NO released to the NOA.

Confocal imaging of UCNPs in live tumor spheroids

Spheroids were grown and incubated with macrophages with and without particles as described in a previous section. Calcein AM (10 μM) was incubated with the spheroids for 2 h in DMEMpy and to mark spheroid peripheries. Live spheroids were added to a Petri dish with HBSS. UCNPs were detected using a 3 W 100 fs pulsed laser (37.5 nJ per pulse) operating at 810 nm. Images were acquired with an Olympus Flowview 1000MPE confocal microscope with a 25× objective (numerical aperture = 1.05). Images were recorded over a 508.431 μm × 508.431 μm area (1024 × 1024 pixels) and were acquired with a scan rate of 100 μs per pixel. Bandpass filters (420–460 nm and 495–540) nm were utilized to isolate fluorescence from UCNPs and calcein AM, respectively. Images acquired every 10 μm were combined to form 3D reconstructions with ImageJ.

Tumoricidal potential of high dose NO therapy

Five spheroids containing microparticle loaded macrophages with and without NO-donor were transferred to the corner of a cuvette containing DMEMpy. Spheroids were exposed to a 794 nm laser at 13.1 W cm^{-2} for 6 min to release NO from particles inside macrophages in the spheroids. This procedure was done to each spheroid 1, 2, or 3 times with 2 min between each exposure. The spheroids were transferred to a 96 TC-treated well plate and incubated for 24 h. After incubation, media was removed and 100 μL of DPBS was added to each well. To measure spheroid viability, a PNPP assay was used as previously described with slight modifications.[51] Briefly, one 10 mg PNPP substrate tablet was added to 5 mL of a solution containing 0.1 M sodium acetate and 0.1% Triton™ X-100. A 100 μL aliquot of this solution was added to the DPBS already in each well. The plate was incubated at 37 °C for 3–3.5 h. NaOH (10 μL, 1 M) was added to each well after which absorbance was measured at 405 nm on a TECAN M220 Infinite Pro plate reader within 10 min of NaOH addition to prevent loss of signal.

Tumor microenvironment modulation with low dose NO therapy

Spheroids with particle loaded macrophages were transferred to a 96 well TC-treated plate with a pipette and were incubated for 12 h to allow them to adhere. Half of the spheroids were then exposed to a 735 nm LED at 0.58 mW cm^{-2} for 8.5 h. Spheroids were collected in groups of 6 and washed once with DPBS. Accumax™ (300 μL) was added and spheroids were incubated for 30–45 min. Spheroids were broken up with rapid pipetting to form a single cell suspension. Cells were fixed with 4% paraformaldehyde (PFA) for 10 min followed by permeabilization with ice cold methanol (MeOH) for 10 min to allow for antibody labeling. Cells were washed three times with DPBS with 1% BSA and 0.1% Tween 20. Rabbit anti-HIF-1α (1 : 100, #PA1-16601; ThermoFisher Scientific) in 1% w/v BSA and 0.1% Tween 20 was added to the cells for 1 h at RT. Cells were washed once with DPBS with 1% BSA and 0.1% Tween 20. FITC labeled goat-anti-rabbit IgG (H + L) (1 : 250, #A27034; ThermoFisher Scientific) was added to the cells for 30 min in DPBS with 1% BSA and 0.1% Tween 20. Cells were washed with DPBS 3 times and analyzed *via* flow cytometry on a FACSAria (Becton Dickinson) using 488 nm (HIF-1α) or 633 nm (CellTracker Deep Red) excitation. Cells were analyzed for % of the cells with fluorescence signal greater than background by setting the gate to exclude the signal from unstained cells (negative control). Results were analyzed with FCM Express 6 Plus.

Conflicts of interest

The authors M. A. Evans, P.-J. Huang, P. C. Ford and S. Mitragotri have submitted a patent application based on aspects of the reported studies. The patent application is owned by the University of California.

Acknowledgements

This research was supported by grants to PCF from the Chemistry Division of the National Science Foundation (CHE-1565702) and to SM from the Department of the Defense, Defense Threat Reduction Agency (HDTRA1-15-1-0045). We thank Aaron Anselmo, Renwei Chen, Megan Chui, John V. Garcia, Vinu Krishnan, Elizabeth S. Levy, Agustin Pierri, Ivan Pina and Anusha Pulusari of the University of California, Santa Barbara, who carried out preliminary studies or provided technical help that advanced our understanding of the systems reported here. UCNPs synthesis at the Molecular Foundry was supported by the Office of Science, Office of Basic Energy Sciences, of the U.S. Department of Energy under Contract No. DE-AC02-05CH11231. Plate reader, dynamic light scattering, and tissue culture work were conducted in the Biological Nanostructures Laboratory within the California NanoSystems Institute, supported by the University of California, Santa Barbara and the University of California, Office of the President. We acknowledge the use of the NRI-MCDB Microscopy Facility and its single and multiphoton spectral laser scanning confocal and supported by the Office of The Director, National Institutes of Health of the NIH under Award # S10OD010610 and S10RR02259501A1. Inductively coupled plasma atomic emission spectroscopic measurements were conducted in the UCSB MRL Shared Experimental Facilities which are supported by the MRSEC Program of the NSF under Award No. DMR-1720256; a member of the NSF-funded Materials Research Facilities Network.

Notes and references

§ A reviewer raised the legitimate concern that Gd^{3+} has been shown to be toxic to humans. Inclusion of the Gd^{3+} dopant in the UCNPs in the present case was purely

for synthetic convenience, since the only function Gd^{3+} serves is to facilitate synthesis of the desired hexagonal phase of $NaYF_4$ (ref. 34–36). There are other methods for synthesizing hexagonal $NaYF_4$ without Gd (ref. 33), and these will be used in future studies.

1 (*a*) L. A. Ridnour, D. D. Thomas, C. Switzer, W. Flores-Santana, J. S. Isenberg, S. Ambs, D. D. Roberts and D. A. Wink, Molecular Mechanisms for Discrete Nitric Oxide Levels in Cancer, *Nitric Oxide*, 2008, **19**, 73–76; (*b*) S. Mocellin, V. Bronte and D. Nitti, Nitric Oxide, a Double-Edged Sword in Cancer Biology: Searching for Therapeutic Opportunities, *Med. Res. Rev.*, 2007, **27**, 317–352.

2 D. D. Thomas, Z. P. Liu, S. P. Kantrow and J. R. Lancaster, The Biological Lifetime of Nitric Oxide: Implications for the Perivascular Dynamics of NO and O_2, *Proc. Natl. Acad. Sci. U. S. A.*, 2001, **98**, 355–360.

3 L. R. Makings and R. Y. Tsien, Caged Nitric Oxide-Stable Organic Molecules from Which NO can be Photoreleased, *J. Biol. Chem.*, 1994, **269**, 6282–6285.

4 N. J. Farrer, L. Salassa and P. J. Sadler, Photoactivated Chemotherapy (PACT): The Potential of Excited-State D-Block Metals in Medicine, *Dalton Trans.*, 2009, 10690–10701.

5 M. A. Sgambellone, A. David, R. N. Garner, K. R. Dunbar and C. Turro, Cellular Toxicity Induced by the Photorelease of a Caged Bioactive Molecule: Design of a Potential Dual-Action Ru(II) Complex, *J. Am. Chem. Soc.*, 2013, **135**, 11274–11282.

6 A. Leonidova, V. Pierroz, R. Rubbiani, Y. Lan, A. G. Schmitz, A. Kaech, R. K. O. Sigel, S. Ferrari and G. Gasser, Photo-Induced Uncaging of a Specific Re(I) Organometallic Complex in Living Cells, *Chem. Sci.*, 2014, **5**, 4044–4056.

7 A. E. Pierri, D. A. Muizzi, A. D. Ostrowski and P. C. Ford, Photo-Controlled Release of NO and CO with Inorganic and Organometallic Complexes, *Structure and Bonding*, 2015, **165**, 1–45.

8 (*a*) P. C. Ford, Photochemical Delivery of Nitric Oxide, *Nitric Oxide*, 2013, **34**, 56–64; (*b*) P. C. Ford, From Curiosity to Applications. A Personal Perspective on Inorganic Photochemistry, *Chem. Sci.*, 2016, **7**, 2964–2986.

9 L. A. Buldt and O. S. Wenger, Chromium Complexes for Luminescence, Solar Cells, Photoredox Catalysis, Upconversion, and Phototriggered NO Release, *Chem. Sci.*, 2017, **8**, 7359–7367.

10 S. Sortino, Light-Controlled Nitric Oxide Delivering Molecular Assemblies, *Chem. Soc. Rev.*, 2010, **39**, 2903–2913.

11 R. A. Weissleder, Clearer Vision for *in vivo* Imaging, *Nat. Biotechnol.*, 2001, **19**, 316–317.

12 K. König, Multiphoton Microscopy in Life Sciences, *J. Microsc.*, 2000, **200**, 83–104.

13 Y. Hitomi, Y. Iwamoto and M. Kodera, Electronic Tuning of Nitric Oxide Release from Manganese Nitrosyl Complexes by Visible Light Irradiation: Enhancement of Nitric Oxide Release Efficiency by the Nitro-Substituted Quinoline Ligand, *Dalton Trans.*, 2013, **43**, 2161–2167.

14 A. A. Eroy-Reveles, Y. Leung, C. M. Beavers, M. M. Olmstead and P. K. Mascharak, Near-Infrared Light Activated Release of Nitric Oxide from Designed Photoactive Manganese Nitrosyls: Strategy, Design, and Potential as NO Donors, *J. Am. Chem. Soc.*, 2008, **130**, 4447–4458.

15 P. C. Ford, Polychromophoric Metal Complexes for Generating the Bioregulatory Agent Nitric Oxide by Single- and Two-Photon Excitation, *Acc. Chem. Res.*, 2008, **41**, 190–200.

16 P. T. Burks, J. V. Garcia, R. GonzalezIrias, J. T. Tillman, M. Niu, A. A. Mikhailovsky, J. Zhang, F. Zhang and P. C. Ford, Nitric Oxide Releasing Materials Triggered by Near-Infrared Excitation Through Tissue Filters, *J. Am. Chem. Soc.*, 2013, **135**, 18145–18152.

17 R. R. Guo, Y. Tian, Y. Wang and W. Yang, Near-Infrared Laser-Triggered Nitric Oxide Nanogenerators for the Reversal of Multidrug Resistance in Cancer, *Adv. Funct. Mater.*, 2017, **27**, #1606398.

18 E. S. Levy, D. P. Morales, J. V. Garcia, N. O. Reich and P. C. Ford, Near-IR Mediated Intracellular Uncaging of NO from Cell Targeted Hollow Gold Nanoparticles, *Chem. Commun.*, 2015, **51**, 17692–17695.

19 R. K. Jain and T. Stylianopoulos, Delivering Nanomedicine to Solid Tumors, *Nat. Rev. Clin. Oncol.*, 2010, **7**, 653–664.

20 J. Fang, H. Nakamura and H. Maeda, The EPR Effect. Unique Features of Tumor Blood Vessels for Drug Delivery, Factors Involved and Limitations and Augmentation of the Effect, *Adv. Drug Delivery Rev.*, 2011, **63**, 136–151.

21 T. Lammers, F. Kiessling, W. E. Hennink and G. Storm, Drug Targeting to Tumors: Principles, Pitfalls and (pre-)clinical progress, *J. Controlled Release*, 2012, **161**, 175–187.

22 C. Murdoch, A. Giannoudis and C. E. Lewis, Mechanisms Regulating the Recruitment of Macrophages into Hypoxic Areas of Tumors and Other Ischemic Tissues, *Blood*, 2004, **104**, 2224–2234.

23 M. R. Choi, K. J. Stanton-Maxey, J. K. Stanley, C. S. Levin, R. Bardhan, D. Akin, S. Badve, J. Sturgis, J. P. Robinson, R. Bashir, N. J. Halas and S. E. Clare, A Cellular Trojan Horse for Delivery of Therapeutic Nanoparticles into Tumors, *Nano Lett.*, 2007, **7**, 3759–3765.

24 N. Doshi, A. J. Swiston, J. B. Gilbert, M. L. Alcaraz, R. E. Cohen, M. F. Rubner and S. Mitragotri, Cell-Based Drug Delivery Devices Using Phagocytosis-Resistant Backpacks, *Adv. Mater.*, 2011, **23**, H105–H109.

25 A. C. Anselmo and S. Mitragotri, Cell-Mediated Delivery of Nanoparticles: Taking Advantage of Circulatory Cells to Target Nanoparticles, *J. Controlled Release*, 2014, **190**, 531–541.

26 J. Choi, H. Y. Kim, E. J. Ju, J. Jung, J. Park, H. K. Chung, J. S. Lee, H. J. Park, S. Y. Song, S. Y. Jeong and E. K. Choi, Use of Macrophages to Deliver Therapeutic and Imaging Contrast Agents to Tumors, *Biomaterials*, 2012, **33**, 4195–4203.

27 W. C. Huang, M. Y. Shen, H. H. Chen, S. C. Lin, W. H. Chiang, P. H. Wu, C. W. Chang, C. S. Chiang and H. C. Chiu, Monocytic Delivery of Therapeutic Oxygen Bubbles for Dual-Modality Treatment of Tumor Hypoxia, *J. Controlled Release*, 2015, **220**(part B), 738–750.

28 W. C. Huang, W. H. Chiang, Y. H. Cheng, W. C. Lin, C. F. Yu, C. Y. Yen, C. K. Yeh, C. S. Chern, C. S. Chiang and H. C. Chiu, Tumortropic Monocyte-Mediated Delivery of Echogenic Polymer Bubbles and Therapeutic Vesicles for

Chemotherapy of Tumor Hypoxia, *Biomaterials*, 2015, **71**(suppl. C), 71–83.

29 Y. F. Wang, G. Y. Liu, L. D. Sun, J. W. Xiao, J. C. Zhou and C. H. Yan, Nd^{3+}-Sensitized Upconversion Nanophosphors: Efficient *In Vivo* Bioimaging Probes with Minimized Heating Effect, *ACS Nano*, 2013, **7**, 7200–7206.

30 J. V. Garcia, F. Zhang and P. C. Ford, Multi-Photon Excitation in Uncaging the Small Molecule Bioregulator Nitric Oxide, *Philos. Trans. R. Soc., A*, 2013, **371**, 20120129/1–20120129/25.

31 E. S. Levy, C. A. Tajon, T. S. Bischof, J. Iafrati, A. Fernandez-Bravo, D. J. Garfield, M. Chamanzar, M. M. Maharbiz, V. S. Sohal, P. J. Schuck, B. E. Cohen and E. M. Chan, Energy-Looping Nanoparticles: Harnessing Excited-State Absorption for Deep-Tissue Imaging, *ACS Nano*, 2016, **10**, 8423–8433.

32 X. Xie, N. Gao, R. Deng, Q. Sun, Q. H. Xu and X. Liu, Mechanistic Investigation of Photon Upconversion in Nd^{3+}-Sensitized Core–Shell Nanoparticles, *J. Am. Chem. Soc.*, 2013, **135**, 12608–12611.

33 A. D. Ostrowski, E. M. Chan, D. J. Gargas, E. M. Katz, G. Han, P. J. Schuck, D. J. Milliron and B. E. Cohen, Controlled Synthesis and Single-Particle Imaging of Bright, Sub-10 nm Lanthanide-Doped Upconverting Nanocrystals, *ACS Nano*, 2012, **6**, 2686–2692.

34 F. Wang, Y. Han, C. S. Lim, Y. Lu, J. Wang, J. Xu, H. Chen, C. Zhang, M. Hong and X. Liu, Simultaneous Phase and Size Control of Upconversion Nanocrystals through Lanthanide Doping, *Nature*, 2010, **463**, 1061–1065.

35 G. S. Yi and G. M. Chow, Synthesis of Hexagonal-Phase $NaYF_4$:Yb,Er and $NaYF_4$:Yb,Tm Nanocrystals with Efficient Up-Conversion Fluorescence, *Adv. Funct. Mater.*, 2006, **16**, 2324–2329.

36 Y. Zhao, Q. Zhan, J. Liu and S. He, Optically Investigating Nd^{3+}–Yb^{3+} Cascade Sensitized Upconversion Nanoparticles for High Resolution, Rapid Scanning, Deep and Damage-Free Bio-Imaging, *Biomed. Opt. Express*, 2015, **6**, 838–848.

37 T. G. Park, H. Yong Lee and Y. A. Sung Nam, New Preparation Method for Protein Loaded Poly(D,L-Lactic-Co-Glycolic Acid) Microspheres and Protein Release Mechanism Study, *J. Controlled Release*, 1998, **55**, 181–191.

38 M. F. Zambaux, F. Bonneaux, R. Gref, P. Maincent, E. Dellacherieb, M. J. Alonso, P. Labrude and C. Vigneron, Influence of Experimental Parameters on the Characteristics of Poly(Lactic Acid) Nanoparticles Prepared by a Double Emulsion Method, *J. Controlled Release*, 1998, **50**, 31–40.

39 J. A. Champion, Y. K. Katare and S. Mitragotri, Particle Shape: A New Design Parameter for Micro- and Nanoscale Drug Delivery Carriers, *J. Controlled Release*, 2007, **121**, 3–9.

40 J. V. Garcia, J. Yang, D. Shen, C. Yao, X. Li, R. Wang, G. D. Stucky, D. Zhao, P. C. Ford and F. Zhang, NIR-Triggered Release of Caged Nitric Oxide Using Upconverting Nanostructured Materials, *Small*, 2012, **8**, 3800–3805.

41 J. A. Champion and S. Mitragotri, Role of Target Geometry in Phagocytosis, *Proc. Natl. Acad. Sci. U. S. A.*, 2006, **103**, 4930–4934.

42 K. A. Beningo and Y. Wang, Fc-Receptor-Mediated Phagocytosis Is Regulated by Mechanical Properties of the Target, *J. Cell Sci.*, 2002, **115**, 849–856.

43 A. Gnach, T. Lipinski, A. Bednarkiewicz, J. Rybkaab and J. A. Capobianco, Upconverting nanoparticles: Assessing the Toxicity, *Chem. Soc. Rev.*, 2015, **44**, 1561–1584.

44 S. Pfeiffer, E. Leopold, K. Schmidt, F. Brunner and B. Mayer, Inhibition of Nitric Oxide Synthesis by NG-Nitro-L-Arginine Methyl Ester (L-NAME): Requirement for Bioactivation to the Free Acid, NG-Nitro-L-Arginine, *Br. J. Pharmacol.*, 1996, **118**, 1433–1440.

45 Y. Chen and L. Liu, Modern Methods for Delivery of Drugs across the Blood-brain Barrier, *Adv. Drug Delivery Rev.*, 2012, **64**, 640–665.

46 Y. N. Chang, H. Guo, J. Li, Y. Song, M. Zhang, J. Jin, G. Xing and Y. Zhao, Adjusting the Balance between Effective Loading and Vector Migration of Macrophage Vehicles to Deliver Nanoparticles, *PLoS One*, 2013, **8**, e76024.

47 P. S. Jiang, C. F. Yu, C. Y. Yen, C. W. Woo, S. H. Lo, Y. K. Huang, J. H. Hong and C. S. Chiang, Irradiation Enhances the Ability of Monocytes as Nanoparticle Carrier for Cancer Therapy, *PLoS One*, 2015, **10**, e0139043.

48 D. L. Priwitaningrum, J. B. G. Blondé, A. Sridhar, J. van Baarlen, W. E. Hennink, G. Storm, S. Le Gac and J. Prakash, Tumor Stroma-Containing 3D Spheroid Arrays: A Tool to Study Nanoparticle Penetration, *J. Controlled Release*, 2016, **244**(part B), 257–268.

49 T. Silzle, M. Kreutz, M. A. Dobler, G. Brockhoff, R. Knuechel and L. A. Kunz-Schughart, Tumor-Associated Fibroblasts Recruit Blood Monocytes into Tumor Tissue, *Eur. J. Immunol.*, 2003, **33**, 1311–1320.

50 J. M. Brown, Tumor Hypoxia in Cancer Therapy, *Methods Enzymol.*, 2007, **435**, 295–321.

51 J. Friedrich, W. Eder, J. Castaneda, M. Doss, E. Huber, R. Ebner and L. A. Kunz-Schughart, A Reliable Tool to Determine Cell Viability in Complex 3-D Culture: The Acid Phosphatase Assay, *J. Biomol. Screening*, 2007, **12**, 925–937.

52 A. Yerlikaya, E. Okur and E. Ulukaya, The p53-Independent Induction of Apoptosis in Breast Cancer Cells in Response to Proteasome Inhibitor Bortezomib, *Tumor Biol.*, 2012, **33**, 1385–1392.

53 D. D. Thomas, M. G. Espey, L. A. Ridnour, L. J. Hofseth, D. Mancardi, C. C. Harris and D. A. Wink, Hypoxic Inducible Factor 1α, Extracellular Signal-Regulated Kinase, and p53 Are Regulated by Distinct Threshold Concentrations of Nitric Oxide, *Proc. Natl. Acad. Sci. U. S. A.*, 2004, **101**, 8894–8899.

54 J. Mateo, M. García-Lecea, S. Cadenas, C. Hernández and S. Moncada, Regulation of Hypoxia-Inducible Factor-1α by Nitric Oxide through Mitochondria-Dependent and -Independent Pathways, *Biochem. J.*, 2003, **376**, 537–544.

55 H. Yasuda, Solid Tumor Physiology and Hypoxia-Induced Chemo/Radio-Resistance: Novel Strategy for Cancer Therapy: Nitric Oxide Donor as a Therapeutic Enhancer, *Nitric Oxide*, 2008, **19**, 205–216.

56 G. N. Masoud and W. Li, HIF-1α Pathway: Role, Regulation and Intervention for Cancer Therapy, *Acta Pharm. Sin. B*, 2015, **5**, 378–389.

57 T. Q. Lang, X. Dong, Y. Huang, W. Ran, Q. Yin, P. C. Zhang, Z. Zhang, H. Yu and Y. Li, Ly6C^{hi} Monocytes Delivering pH-Sensitive Micelle Loading Paclitaxel Improve Targeting Therapy of Metastatic Brest Cancer, *Adv. Funct. Mater.*, 2017, **27**, 1–11.

58 J. B. Mitchell, D. A. Wink, W. DeGraff, J. Gamson, L. K. Keefer and M. C. Krishna, Hypoxic Mammalian Cell Radiosensitization by Nitric Oxide, *Cancer Res.*, 1993, **53**, 5845–5848.

59 J. Bourassa, W. DeGraff, S. Kudo, D. A. Wink, J. B. Mitchell and P. C. Ford, Photochemistry of Roussin's Red Salt, $Na_2[Fe_2S_2(NO)_4]$, and of Roussin's Black Salt, $NH_4[Fe_4S_3(NO)_7]$. *In Situ* Nitric Oxide Generation to Sensitize γ-Radiation Induced Cell Death, *J. Am. Chem. Soc.*, 1997, **119**, 2853–2860.

60 X. Zhang, R. Goncalves and D. M. Mosser, The Isolation and Characterization of Murine Macrophages, *Curr. Protoc. Immunol.*, 2008, **83**, 14.1.1–14.1.14.

61 F. M. Marim, T. N. Silveira, D. S. Lima Jr and D. S. Zamboni, A Method for Generation of Bone Marrow-Derived Macrophages from Cryopreserved Mouse Bone Marrow Cells, *PLoS One*, 2010, **5**, e15263.

62 D. M. Wuest, A. M. Wing and L. H. Lee, Membrane Configuration Optimization for a Murine *in Vitro* Blood-brain Barrier Model, *J. Neurosci. Methods*, 2013, **212**, 211–221.